AD-A183 566 ADVANCED PROCESSING AND PROPERTIES OF HIGH-PERFORMANCE ALLOYS(U) PENNSYLVANIA STATE UNIV UNIVERSITY PARK DEPT OF MATERIALS SCIENCE AND ENGINEERING D A KOSS FEB 87 1/1

UNCLASSIFIED N00014-86-K-0301 F/G 11/6 NL

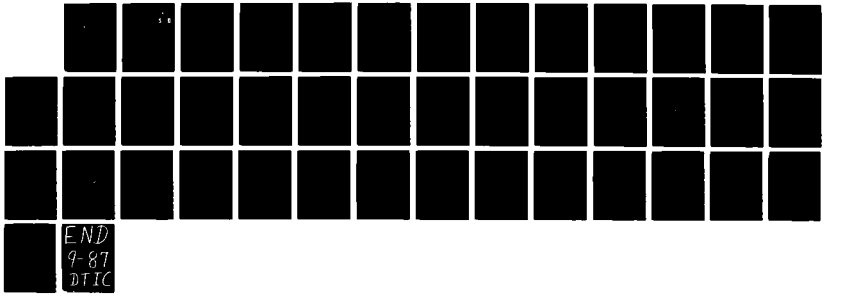

END
9-87
DTIC

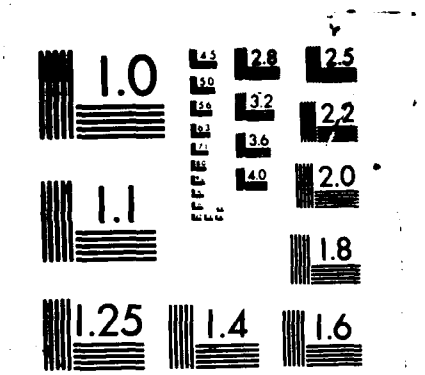


MICROCOPY RESOLUTION TEST CHART
NATIONAL BUREAU OF STANDARDS-1963-A

AD-A183 566

DTIC FILE COPY

DTIC ELECTE AUG 2 0 1987 S D

TECHNICAL REPORT NO. 6

TO

THE OFFICE OF NAVAL RESEARCH
CONTRACT NO. N00014-86-K-0381

# ADVANCED PROCESSING AND PROPERTIES OF HIGH PERFORMANCE ALLOYS

D. A. Koss

DEPARTMENT OF MATERIALS SCIENCE AND ENGINEERING
THE PENNSYLVANIA STATE UNIVERSITY
UNIVERSITY PARK, PA 16802

REPORT FOR THE PERIOD 1 MAY 1986 - 31 JANUARY 1987

RUTH H. HOOKER TECHNICAL LIBRARY 1987

REPRODUCTION IN WHOLE OR IN PART IS PERMITTED
FOR ANY PURPOSE OF THE UNITED STATES GOVERNMENT.
DISTRIBUTION OF THIS DOCUMENT IS UNLIMITED.

87 8 3 029

SECURITY CLASSIFICATION OF THIS PAGE (When Data Entered)

## REPORT DOCUMENTATION PAGE

READ INSTRUCTIONS BEFORE COMPLETING FORM

| | |
|---|---|
| 1. REPORT NUMBER: Technical Report No. 6 | 2. GOVT ACCESSION NO.: ADA183560 |
| 3. RECIPIENT'S CATALOG NUMBER: | |
| 4. TITLE (and Subtitle): Advanced Processing and Properties of High Performance Alloys | 5. TYPE OF REPORT & PERIOD COVERED: |
| | 6. PERFORMING ORG. REPORT NUMBER: |
| 7. AUTHOR(s): D. A. Koss | 8. CONTRACT OR GRANT NUMBER(s): N00014-86-K-0381 |
| 9. PERFORMING ORGANIZATION NAME AND ADDRESS: Department of Materials Science and Engineering<br>The Pennsylvania State University<br>University Park, PA 16802 | 10. PROGRAM ELEMENT, PROJECT, TASK AREA & WORK UNIT NUMBERS: |
| 11. CONTROLLING OFFICE NAME AND ADDRESS: Office of Naval Research<br>800 N. Quincy St.<br>Arlington, VA 22217 | 12. REPORT DATE: February 1987 |
| | 13. NUMBER OF PAGES: 38 |
| 14. MONITORING AGENCY NAME & ADDRESS (if different from Controlling Office): | 15. SECURITY CLASS. (of this report): Unclassified |
| | 15a. DECLASSIFICATION/DOWNGRADING SCHEDULE: |

16. DISTRIBUTION STATEMENT (of this Report)

Distribution of this document is unlimited.

17. DISTRIBUTION STATEMENT (of the abstract entered in Block 20, if different from Report)

18. SUPPLEMENTARY NOTES

19. KEY WORDS (Continue on reverse side if necessary and identify by block number)

Processing, Fracture mechanisms, Void/Pore linking, low cycle fatigue, rapidly solidified alloys, Ti alloys, hot isostatic pressing (HIP), strain-path effects.

20. ABSTRACT (Continue on reverse side if necessary and identify by block number)

Progress is reviewed for a research program whose purpose is to establish a broad-based understanding of the application and consequences of advanced processing techniques, especially as they influence the strength and fracture resistance of high performance structural alloys. While some of the research is specific to a certain alloy systems, many aspects of the program constitute fundamental studies of the deformation and fracture of engineering alloys containing processing - induced defects. Progress for the period May 1, 1986

DD FORM 1 JAN 73 1473 EDITION OF 1 NOV 65 IS OBSOLETE

S/N 0102-LF-014-6601

SECURITY CLASSIFICATION OF THIS PAGE (When Data Entered)

to January 31, 1987 is reviewed for the following projects within the program:

(1) the mechanism of void/pore linking in ductile fracture,

(2) the influence of porosity on low cycle fatigue,

(3) the deformation of rapidly solidified Ti alloys at elevated temperatures,

(4) strain-path effects on fracture, and

(5) hot isostatic pressing of metallic powders. (Keywords) →

DTIC
COPY
INSPECTED
6

Accesion For
NTIS CRA&I ☒
DTIC TAB ☐
Unannounced ☐
Justification
By
Distribution/
Availability Codes
Dist Avail and/or special
A-1

## INSTRUCTIONS FOR PREPARATION OF REPORT DOCUMENTATION PAGE

RESPONSIBILITY. The controlling DoD office will be responsible for completion of the Report Documentation Page, DD Form 1473, in all technical reports prepared by or for DoD organizations.

CLASSIFICATION. Since this Report Documentation Page, DD Form 1473, is used in preparing announcements, bibliographies, and data banks, it should be unclassified if possible. If a classification is required, identify the classified items on the page by the appropriate symbol.

### COMPLETION GUIDE

General. Make Blocks 1, 4, 5, 6, 7, 11, 13, 15, and 16 agree with the corresponding information on the report cover. Leave Blocks 2 and 3 blank.

Block 1. *Report Number. Enter the unique alphanumeric report number shown on the cover.*

Block 2. Government Accession No. Leave Blank. This space is for use by the Defense Documentation Center.

Block 3. Recipient's Catalog Number. Leave blank. This space is for the use of the report recipient to assist in future retrieval of the document.

Block 4. Title and Subtitle. Enter the title in all capital letters exactly as it appears on the publication. Titles should be unclassified whenever possible. Write out the English equivalent for Greek letters and mathematical symbols in the title *(see "Abstracting Scientific and Technical Reports of Defense-sponsored RDT/E," AD-667 000).* If the report has a subtitle, this subtitle should follow the main title, be separated by a comma or semicolon if appropriate, and be initially capitalized. If a publication has a title in a foreign language, translate the title into English and follow the English translation with the title in the original language. Make every effort to simplify the title before publication.

Block 5. Type of Report and Period Covered. Indicate here whether report is interim, final, etc., and, if applicable, inclusive dates of period covered, such as the life of a contract covered in a final contractor report.

Block 6. Performing Organization Report Number. Only numbers other than the official report number shown in Block 1, such as series numbers for in-house reports or a contractor/grantee number assigned by him, will be placed in this space. If no such numbers are used, leave this space blank.

Block 7. Author*(s)*. Include corresponding information from the report cover. Give the name*(s)* of the author*(s)* in conventional order *(for example, John R. Doe or, if author prefers, J. Robert Doe).* In addition, list the affiliation of an author if it differs from that of the performing organization.

Block 8. Contract or Grant Number*(s)*. For a contractor or grantee report, enter the complete contract or grant number*(s)* under which the work reported was accomplished. Leave blank in in-house reports.

Block 9. Performing Organization Name and Address. For in-house reports enter the name and address, including office symbol, of the performing activity. For contractor or grantee reports enter the name and address of the contractor or grantee who prepared the report and identify the appropriate corporate division, school, laboratory, etc., of the author. List city, state, and ZIP Code.

Block 10. Program Element, Project, Task Area, and Work Unit Numbers. Enter here the number code from the applicable Department of Defense form, such as the DD Form 1498, "Research and Technology Work Unit Summary" or the DD Form 1634. "Research and Development Planning Summary," which identifies the program element, project, task area, and work unit or equivalent under which the work was authorized.

Block 11. *Controlling Office Name and Address. Enter the full, official name and address, including office symbol, of the controlling office. (Equates to funding/sponsoring agency. For definition see DoD Directive 5200.20, "Distribution Statements on Technical Documents.")*

Block 12. Report Date. Enter here the day, month, and year or month and year as shown on the cover.

Block 13. Number of Pages. Enter the total number of pages.

Block 14. Monitoring Agency Name and Address *(if different from Controlling Office).* For use when the controlling or funding office does not directly administer a project, contract, or grant, but delegates the administrative responsibility to another organization.

Blocks 15 & 15a. Security Classification of the Report: Declassification/Downgrading Schedule of the Report. Enter in 15 the highest classification of the report. If appropriate, enter in 15a the declassification/downgrading schedule of the report, using the abbreviations for declassification/downgrading schedules listed in paragraph 4-207 of DoD 5200.1-R.

Block 16. Distribution Statement of the Report. Insert here the applicable distribution statement of the report from DoD Directive 5200.20, "Distribution Statements on Technical Documents."

Block 17. Distribution Statement *(of the abstract entered in Block 20, if different from the distribution statement of the report).* Insert here the applicable distribution statement of the abstract from DoD Directive 5200.20, "Distribution Statements on Technical Documents."

Block 18. Supplementary Notes. Enter information not included elsewhere but useful, such as: Prepared in cooperation with . . . Translation of *(or by)* . . . Presented at conference of . . . To be published in . . .

Block 19. Key Words. Select terms or short phrases that identify the principal subjects covered in the report, and are sufficiently specific and precise to be used as index entries for cataloging, conforming to standard terminology. The DoD "Thesaurus of Engineering and Scientific Terms" *(TEST),* AD-672 000, can be helpful.

Block 20. Abstract. The abstract should be a brief *(not to exceed 200 words)* factual summary of the most significant information contained in the report. If possible, the abstract of a classified report should be unclassified and the abstract to an unclassified report should consist of publicly- releasable information. If the report contains a significant bibliography or literature survey, mention it here. For information on preparing abstracts see "Abstracting Scientific and Technical Reports of Defense-Sponsored RDT&E," AD-667 000.

☆ U.S.Government Printing Office:1976—603-813/3890 2-1

# INTRODUCTION

Advanced structural systems require high performance alloys which must exhibit high strength and good fracture resistance over a wide range of temperatures and environments. In recent years, such systems are becoming increasingly materials-limited. This is primarily a result of the small, incremental improvements in properties of such alloys: in addition an escalation of the cost of a finished part has frequently confined the application of high performance alloys to selected critical components. These considerations have caused a demand for the application of advanced processing techniques to the production of high performance alloys both to create new alloys exhibiting large property improvements and/or to reduce the cost of finished component by using near net-shape fabrication methods. One example is application of rapid solidification processing as a method of developing new families of high performance alloys,[1-4] which in turn require extensive processing based on new applications of powder metallurgy techniques.

An underlying problem in high performance alloy technology is that the application of new processing methods to these alloys exceeds the fundamental knowledge base necessary to predict the resulting component behavior in service. Thus, service reliability may be impaired. For example, the materials can contain processing-induced defects, such as porosity or inclusions, which can seriously degrade service reliability especially with regard to fracture. Furthermore, the processing required to achieve a fully dense part usually limits the microstructures available to a component and therefore its properties, especially in the case of rapidly solidified alloys.

The primary purpose of the present research is to provide a broad-based understanding of the applications and consequences of selected advanced processing techniques to high performance alloys. The research ranges in scope

from fundamental studies of void or pore linking during ductile fracture to the high temperature deformation of rapidly solidified, dispersion-strengthened Ti alloys. Much of the research is designed so that it is also a fundamental study of deformation and especially fracture utilizing engineering materials containing processing-induced defects. The present report summarized progress in the areas of research for the period 5/1/86 to 1/31/87 performed under the auspices of Contract No. N00014-86-0381. The research areas may be grouped as follows:

(1) the mechanism of void/pore linking in ductile fracture,

(2) the influence of porosity on low cycle fatigue,

(3) the deformation of rapidly solidified Ti alloys at elevated temperatures,

(4) strain-path effects on fracture, and

(5) hot isostatic pressing of metallic powders.

The educational experience which the above research provides to the graduate students is also significant. The following students have been involved in this program during part or all of the nine month period of this program: Stephen Kampe, Ph.D., January 1987: Barbara Lograsso, Ph.D. candidate: Dale Gerard, Ph.D. candidate; Paul Magnusen, Ph.D. candidate: and Susan Kestner, M.S. May, 1986.

## SUMMARY OF RESEARCH

1. The Mechanism of Void/Pore Linking During Ductile Fracture
[with Paul Magnusen, Ph.D. candidate, Dr. Dave Srolovitz, Los Alamos National Laboratory, Prof. Jong Lee, Michigan technological University].

The ductile fracture of structural alloys by damage accumulation is well known to consist of void nucleation, void growth, and void linking. Of these three stages, the first two have been examined in detail and are reasonably well

understood. While perhaps as important as void nucleation in controlling fracture, void linking remains only poorly understood at best. The present study is the first ever to identify a realistic step-wise sequence of events which results in voids or pores being linking during straining. As such, we believe that this study which is very significant in the understanding of the ductile fracture of solids. Our analysis identifies the critical features of a void/pore distribution as well as the influence of material flow behavior, notably strain hardening. Furthermore, we have successfully simulated the process by modeling void/pore distributions in two dimensions as arrays of circular hole which are characterized by area faction, size, and an "exclusion radius" which controls the degree of clustering. Both experimental and computer simulations have been successfully performed indicating the critical features of the linking process. The following sections describe our progress in this project.

(a) A Physical Model for Void/Pore Linking

Our studies to date indicate the following physical model describes void linking during ductile, microvoid fracture.[5-7] In that model, the void linking process is a consequence of a multi-stage sequence. First, local strain gradients develop near individual holes/pores at small macroscopic strains. Secondly, increasing macroscopic strain localizes strain and triggers flow instabilities on planes of high shear stress between closely spaced and favorably oriented holes/voids. Under plane stress conditions, the instabilities appear to obey a critical thickness strain criterion as in the localized necking in sheet metal over the range of strain paths from uniaxial to plane-strain tension.[8] Although void formation within the localized neck accelerates its development, the onset of the instability is apparently controlled primarily by the strain and stain-rate hardening characteristics of

the material.[17,18,20] Thirdly, the flow instabilities cause failure of the ligament between holes. This creates an elongated hole which, due to its eccentric shape and size, tends also to localize flow along its major axis. The extent of the plastic zone scales with interhole spacing while the strain gradients within the zone are controlled by the strain hardening.[19]

The fourth stage results from the statistical problem or whether or not a third hole/void is located such that it can link to the pair of holes/voids which have linked in the previous stage. If the third hole is favorably located for linking, stages 3 and 4 essentially repeat with the statistics now relating to the location of a fourth hole to the expanded plastic zone of the linked triplet. If a third hole is <u>not</u> favorably located, then macroscopic deformation proceeds until another pair of holes links and stage four of the process repeats. As deformation continues, hole linking results in increased plastic-zone sizes which in turn increase the probability of successive holes/voids being linked. Thus the early stages of void/hole linking occur via localized flow instabilities and fracture of ligaments, linking voids.

As deformation continued but with only a few additional percent of the load-bearing cross section area removed by hole/void linking, the final stage of failure is triggered: an imperfection-initiated general instability[9,10] or the propagation of a crack-like defect. In this fifth stage, a sufficient number of voids/holes have linked to create an imperfection or crack-like defect whose severity increases with strain as the holes link. This triggers a macroscopic shear instability across the remaining cross sectional area of the specimen and generates the large local strains which result in specimen failure by the void sheet mechanism between large voids.

b. Ductile Fracture and Random Vs Regular Hole/Void Arrays

Nearly all previous theories of ductile, microvoid fracture assume a regular distribution of voids/holes and assume an arbitrary, void/hole linking criterion. In a recent study,[7] we have examined the validity of assuming regular arrays of voids by comparing the fracture behavior of specimens containing random and regular arrays of holes. The following indicates some of the conclusions of that study.

(1) Ductile materials containing a random array of holes/voids are less ductile than their regular array counterparts; see Fig. 1 for example. The physical model emphasizes the importance of clustering wherein closely spaced holes or voids can trigger local flow instabilities within the ligaments between holes, subsequently cause hole linking, and eventually lead to percolation. The greater ductility in the specimens containing regular arrays of holes is thus due in large part to the increase in inter-hole spacing.

(2) Increasing the minimum hole spacing $S_m$ between nearest holes in a specimen with a random array increases ductility. Hole linking is retarded by an increase in $S_m$ as greater macroscopic extension is required to increase the extent of the plastic zones near individual holes such that sufficient zone overlap can occur to trigger the instability between holes.

(3) Increasing the hole/void size decreases ductility at a given area fraction and minimum hole spacing. Plastic zones near holes scale with hole size,[11] and thus plastic zone overlap and hole linking occurs at smaller strains between large holes. Thus occurs despite the fact that increasing hole diameter at a given area fraction increases the average hole spacing: a sufficient number of holes/voids are closely spaced such that linking can trigger failure.

(4) Specimens which have low strain hardening and which contain regular arrays of holes are more ductile than their random array counterpart. This

effect is minimal at high strain hardening as is shown for the brass in Figure 1. An obvious factor in this case is the susceptibility of materials with low stain hardening rates to flow instabilities. In a random array with a slightly smaller minimum hole spacing than a regular array, even a small variation in inter-hole spacing will create a cluster of holes which link at smaller strains than the regular array counterpart. In addition, for materials with low strain hardening, the linking of only a few holes/voids will create an imperfection of sufficient severity to cause a macroscopic instability and fracture.[9,10]

(5) Increasing the strain hardening increases the normalized ductility of random arrays. Previous results indicate that flow localization near holes will be more intense in a material of low strain hardening,[12] and also that the critical thickness strain for the onset of localized necking decreases with decreasing strain hardening.[8] Thus the critical strain to trigger hole linking will decrease with decreasing strain-hardening value. It is also well established that once several holes link, imperfection-driven, macroscopic shear instabilities are a sensitive function of strain hardening.[9,10] Specifically, an increase of the strain hardening exponent will delay the onset of the shear instability. Thus the linking of of two holes within a 7075 Al specimen (low strain hole hardening) is sufficient to trigger failure in most of these the high hardening brass specimens require the linking of four holes to cause failure. The brass obviously exhibits greater ductility.

(6) The effects of hole diameter scale with minimum hole spacing. For example, in order to retain the same ductility upon an increase in hole/void size, a concurrent increase in minimum hole spacing is necessary. This effect relates to the scaling of plasticity near (and between) holes with the size of the hole:[11] sp .fically, large holes have correspondingly larger plastic zones.

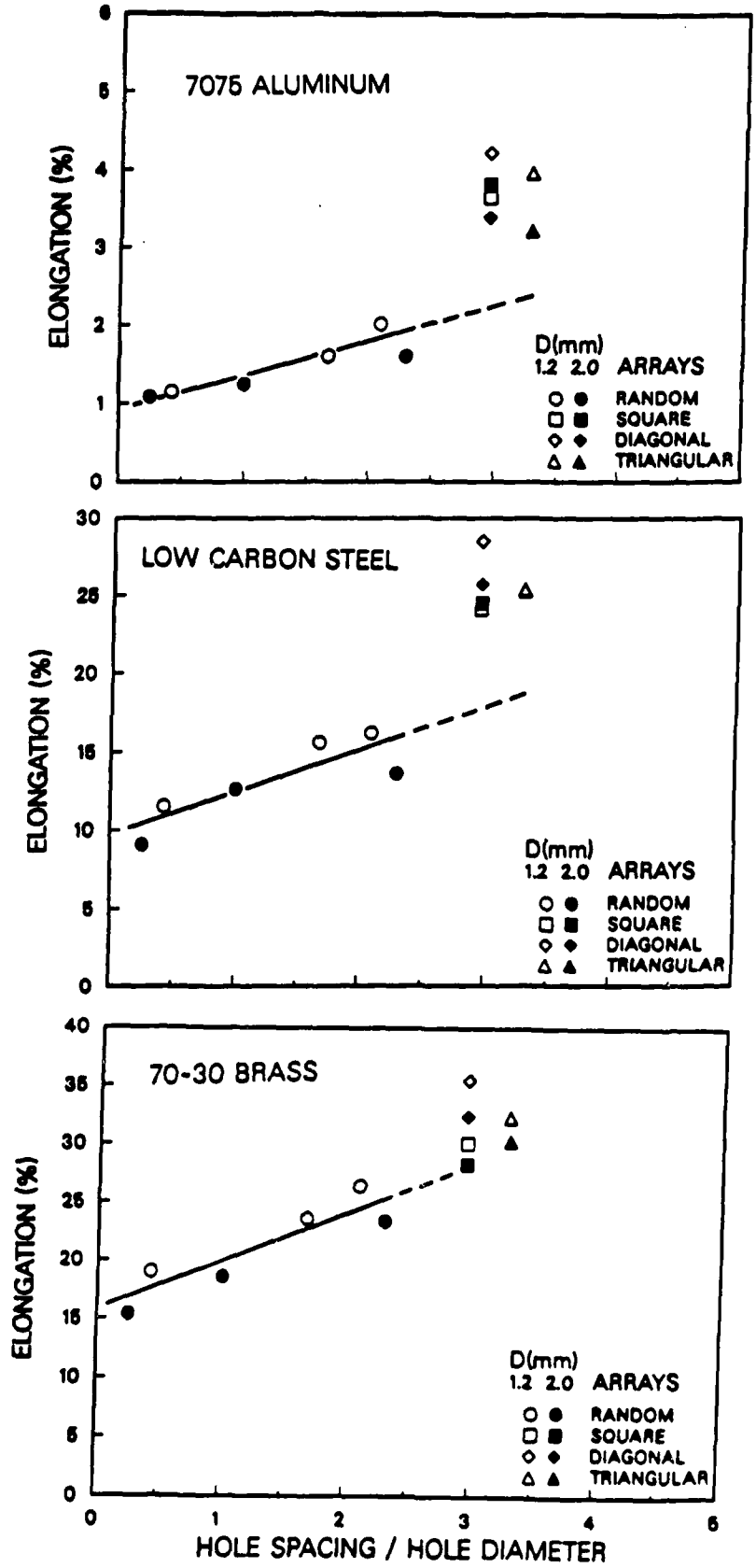


Fig. 1. The dependence of tensile ductility on the ratio of minimum hole spacing to diameter for 7075 Al, low carbon steel and brass sheet specimens containing arrays of holes.

c. A Computer Simulation of Void Linking During Ductile Fracture

As previously mentioned, most existing models of ductile fracture based on the assumption of a regular distribution of voids[13-20] and arbitrary, geometric void linking criterion.[21-23] As a result they rely on an unrealistic void distribution and linking criterion; it is no surprise that they tend to overestimate fracture strains. The present analysis is significant because it relies on the random characteristics of a void/pore distribution and correctly predicts the step-wise nature of the void linking process. As intuitively obvious and as observed experimentally in the modeling studies,[6-8] void linking clearly depends on local plasticity near voids. The simulation therefore relies on an accurate description of the plasticity in a manner consistent with the stepwise linking process described. Specifically, it is necessary to describe analytically those pertinent features of the plastic deformation localized near (a) isolated single holes, (b) pairs of unlinked holes, (c) pairs of linked holes, and (d) multiple holes which have linked (relating to changes of hole geometries due to linking).

Any comprehensive simulation must also account for the dependence of the local plasticity on material parameters, notably strain and strain-rate hardening; in the present study we take into account strain hardening but ignore strain-rate hardening. Given the importance of ligament failure in the presence process, a realistic failure criterion must also be adopted. Finally the simulation must provide an adequate description of a two-dimensional analog of a void/pore microstructure. In this study, the microstructural arrays of equisized, circular holes are analyzed in terms of their (a) size, (b) area fraction, and (c) an "exclusion radius" or "minimum hole spacing" which defines a circular region around a hole within which no other hole may be located.

Step 1 of the void linking process involves the development of local plasticity near isolated holes at small macroscopic strains. In the past year, we have made detailed measurements of the development of local strain gradients in a tensile strain field near isolated holes in 1100-0 aluminum sheet and 70-30 brass sheet.[24] In order that these data may be incorporated into a computer model for simulating ductile fracture, empirical relations were also developed to describe the development of the strain profiles near along a line normal to the tensile axis and passing through the center of an isolated hole, is shown in Figure 2 [11].

Linking of the holes (Step 2 in the Void Linking Process) depends on the manner in which the strain localized between holes/voids. The local thickness strain between a pair of holes prior to linking has been measured along a line normal to the tensile axis passing through the holes. For the range of hole spacings tested, the strain between the holes is observed approximately equal to the sum of the strain due to the two individual holes.

Any simulation of hole/void linking must adapt a realistic criterion for ligament failure. This can be a result of either a strain-driven flow instability or damage accumulation (as in a void-sheet linking of large voids). In the case of simulating two-dimensional modeling of voids by plane-stress (sheet) specimens containing voids, the criterion for hole linking is a critical thickness strain, which is consistent with both instability[8] and accumulated damage failure criteria.[25] For both 1100-0 aluminum and 70-30 brass sheet, the plastic flow between a pair of holes localized at the same value of the local thickness strain: $\varepsilon_{33} = -0.250$. This strain value is independent of the spacing of the holes and the angle of orientation between the holes for the conditions studied.

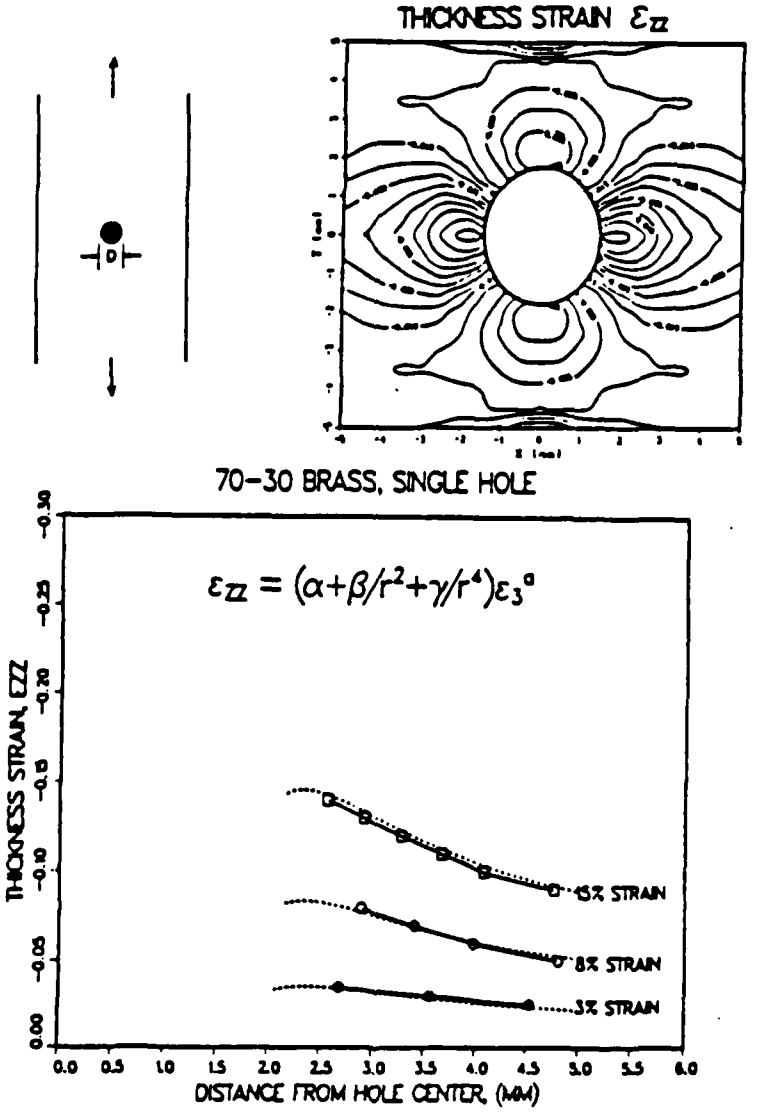


Fig. 2. Thickness strain profiles near a single hole at (a) a macroscopic extensional strain of 0.03 and (b) as a function of the distance from the hole center at y=0. Data are for 70-30 brass.

Once a pair of holes link, two effects occur simultaneous with failure of the ligament. The addition of the ligament as free surface between the holes causes (a) an increase in hole growth rate on an axis parallel to the tensile axis and (b) an abrupt increase in local strain near the holes with no imposed increment in macroscopic strain. This is the essence of Step 2 of the linking process. Both (a) the increase in hole growth and (b) the abrupt increase in local strain have been measured for 1100 Al and 70-30 brass. These data were also fit to empirically determined equations. Of note is the fact that, as expected, the local strain level is greatest when holes spaced far apart link (or several holes on a common line link) in a material of low strain hardening.

In the computer simulation, a macroscopic strain is applied to the material, and in response, a random array of holes elongate and local stain gradients develop near the equisized, cylindrical holes. The strain distribution near holes are replaced in the simulation by the iso-strain contours near the holes as in Fig. 3. These contours approximate the radial distribution of strain at 0.5 $\varepsilon_{33}^{*}$ where $\varepsilon_{33}^{*}$ is the critical thickness strain at ligament failure. Thus, overlap of two zones causes ligament fracture. The elliptical "zones of influence" have a minor axes which lies along the tensile axis and corresponds to the elongated hole diameter.

The simulated sequence of fracture events resulting in failure of a specimen containing a random array of holes (0.05 area fraction of 1.2 mm holes with an exclusion radius of 0.5 mm) is illustrated in Figure 4 for 1100 aluminum. In this figure, the solid ellipses represent the holes which have been elongated with macroscopic strain, and the zones of influence are approximated by the dashed ellipses. It should be recalled that overlap of two zones of influence results in superposition of strains sufficient in magnitude to cause linking of the holes.

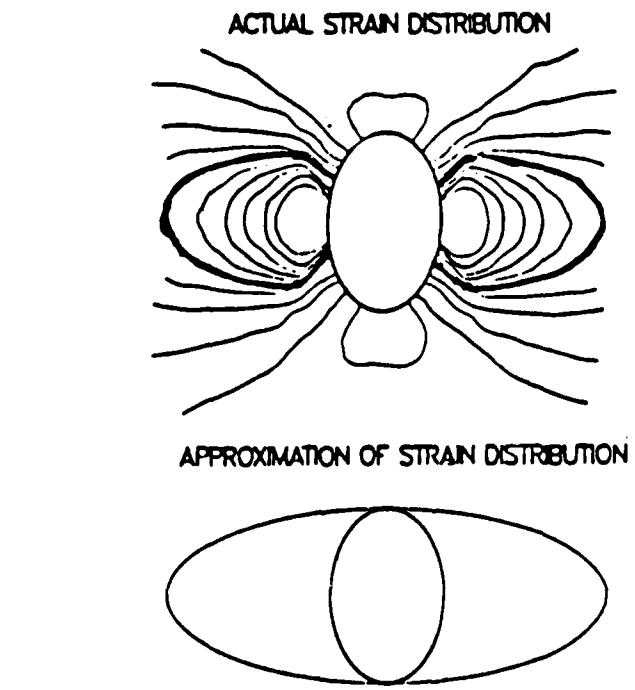


Fig. 3. A schematic of the "zone of influence" shown below an actual strain distribution near an isolated hole. Note that the boundary of the zone of the influence roughly defines a thickness strain of 0.5 $(\varepsilon_{zz})_{crit}$ where $(\varepsilon_{zz})_{crit}$ is the critical thickness strain at the onset of flow instability between holes.

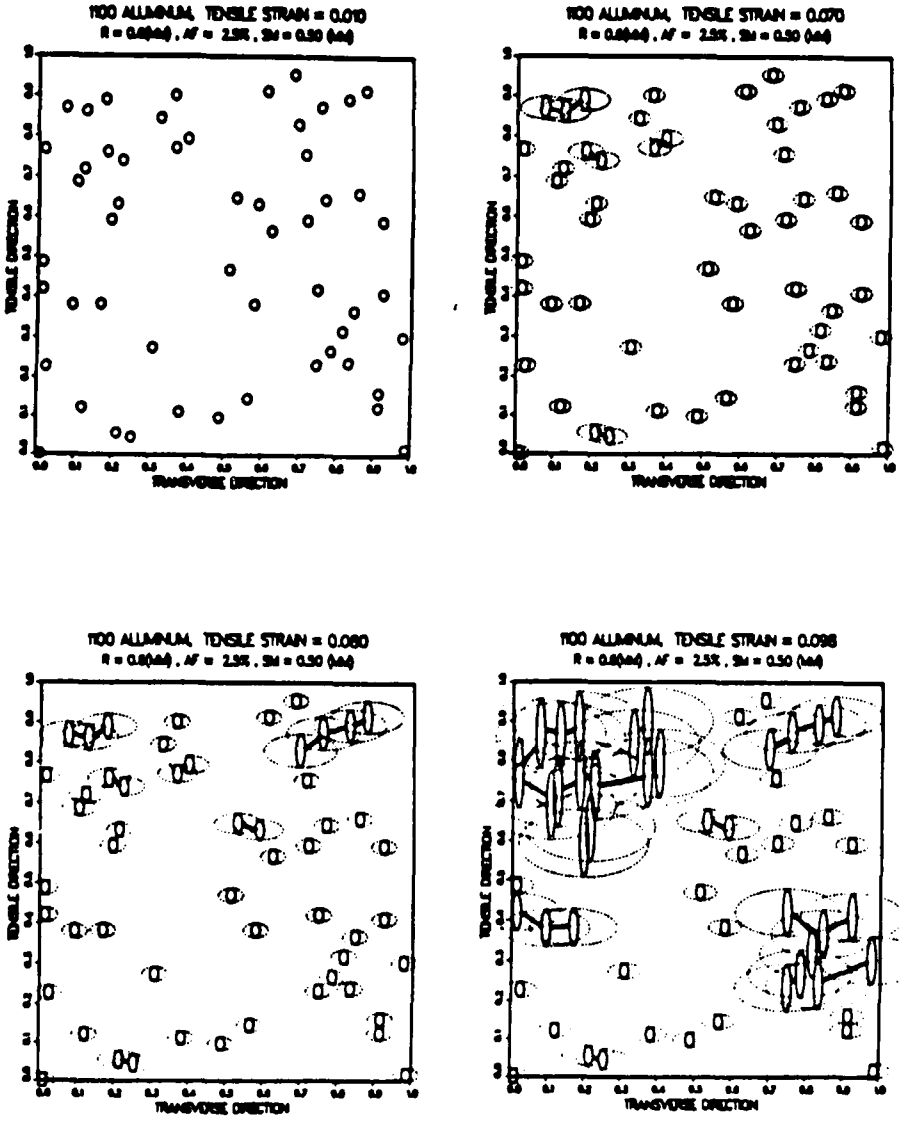


Fig. 4. A computer simulation indicating void growth and linking as modeled in two dimensions using "zones of influence" as a linking criterion.

Examination of Fig. 4 shows that fracture occurs by the sequential, stepwise process previously described for void/hole linking. At small strains, the development of local strain gradients near the holes is evident (Stage 1). With continued straining, flow localization and ligament fracture between closely spaced and favorably oriented holes occurs (Stage 2) and, as shown in Fig. 4, is depicted by overlapping strain contours which are larger than for a single hole due to the amplification effects due to linking. It can be seen in Fig. 4 that if additional holes are not located such that continued linking occurs with the previously linked hole cluster, then deformation proceeds by linking elsewhere in the material (Stage 3). However, when hole linking occurs the increase strain concentration increases the probability of successive linking (Stage 4); the linking of the four holes in the upper right corner of Fig. 4 are good examples of this. Failure of the material occurs at that level of macroscopic strain where the repeated process of hole linking, strain amplification, and additional ligament failure percolates linking across the width of the specimen (Stage 5).

In addition to correctly predicting the hole/void linking sequence, the simulation also predicts accurately the dependence of elongation on the area fraction of holes. This is shown in Fig. 5 for the aluminum and brass specimens. It is important to recognize that agreement between experiment and computer simulation in Fig. 5 is obtained without any adjustable parameters to force a fit. Similar agreement is obtained in analyzing the dependence of fracture strain on the exclusion radius, which measures the degree of clustering in the hole/void array. The simulation also correctly indicates the retardation of hole linking, and increased ductility, in the high strain-hardening brass.

In summary, the step-wise process of void linking in ductile materials is simulated. The analysis is based on two-dimensional modeling of voids as arrays

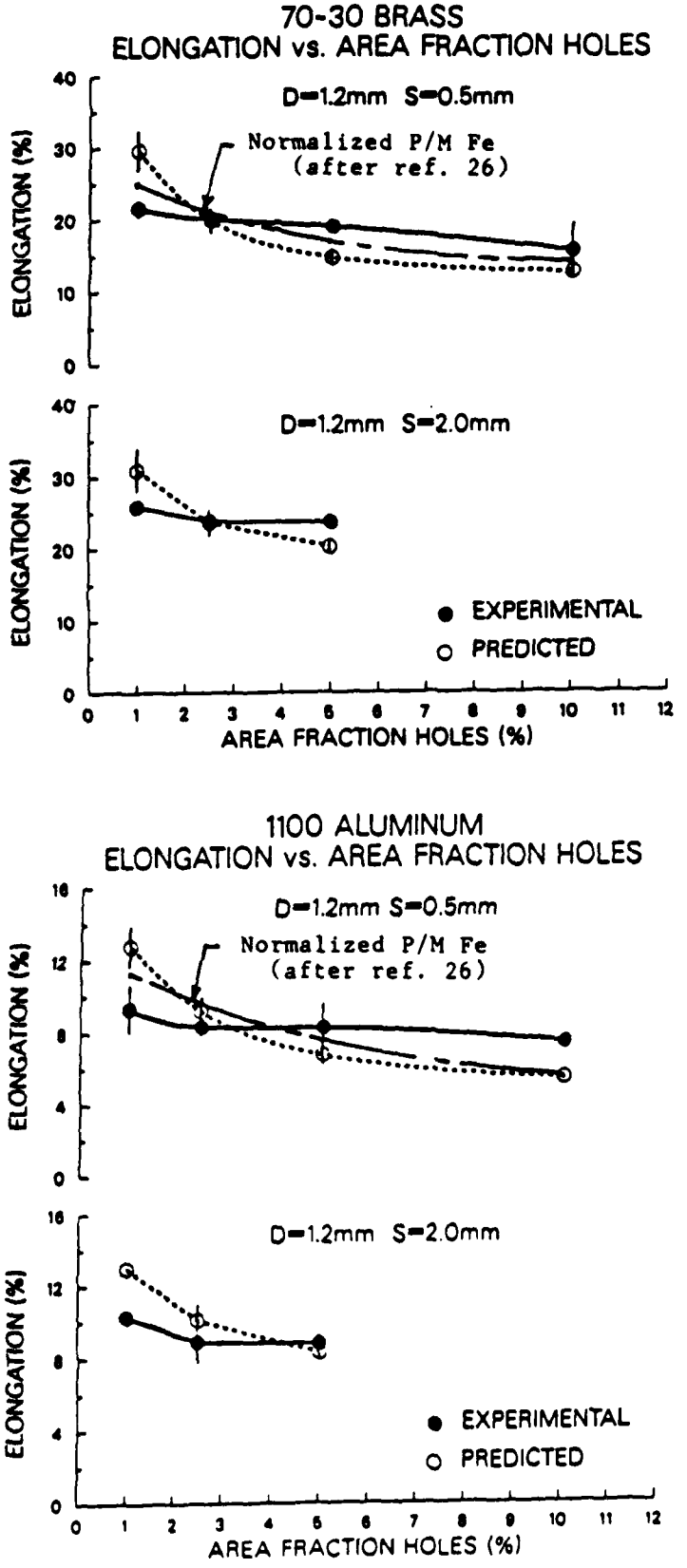


Fig. 5. The dependence of elongation on the area fraction of holes for experimental and computer simulation results. Normalized P/M Fe containing spherical porosity is included for comparison.

of equisized, cylindrical holes characterized by area fraction, hole size, and an exclusion radius. Utilizing experimentally determined strain distributions near holes and a critical thickness strain criterion for hole linking, the simulation depicts the sequential stages of void/pore linking and accurately predicts the experimentally determined fracture strains of specimens containing random arrays of holes. It is significant that the predictions are obtained using only empirically represented experimental data without the use of adjustable parameters to obtain good quantitative agreement with experimental results.

2. The Effects of Porosity on Low Cycle Fatigue [with Dale Gerard, Ph.D. candidate].

The application of powder metallurgy P/M to consolidate high performance alloys often results in inconsistent mechanical behavior as a result of processing-induced defects. A prime source of the inconsistency is the presence of porosity which may be present in a P/M or cast component. The deleterious effects of porosity on high cycle fatigue and tensile ductility is well established.[27] As indicated by our modeling studies, shear localization plays an important role in the linking of pores and the resulting tensile ductility. Thus, it is also expected that the presence of porosity will also have a severe effect on low cycle fatigue, wherein the material is fully plastic and thus susceptible to a pore linking process similar to that previously described for tensile ductility. Unfortunately, there has been no systematic study examining the effects of porosity on low cycle fatigue in a generic manner.

The purpose of this investigation is to determine the effects of porosity and its microstructure (e.g. porosity level, size and shape) on the low cycle

fatigue behavior of powder-processed titanium. Standard P/M processing techniques have been used to prepare specimens containing porosity levels ranging from .5% to 6%, with the 6% porosity level specimens being of two pore size distributions (approximately 25 μm and 60 μm mean diameters).

Fully reversed tension-compression low cycle fatigue tests have been performed to date at room temperature in a total strain control mode at 1.5% total strain. The tests were periodically interrupted for surface replication in order to monitor the low cycle fatigue deformation. The following observations are especially pertinent:

(1) At a given strain amplitude, increasing the pore content significantly decreases the low cycle fatigue life. This effect is more pronounced in specimens containing coarse porosity than in those with fine pores. Fig. 6 shows typical data: note the large loss of life with even a small amount of porosity and the significant effect of pore size at 6% porosity.

(2) As expected, the number of cycles to initiate a microcrack is greatly decreased when porosity is present. As shown in Fig. 7, this effect is especially dramatic when a high level (6%) of coarse porosity is present.

(3) In all cases, greater than 50% of the fatigue life appears to be associated with the linking of microcracks at large strain amplitudes. As shown in Fig. 8, the microcrack linking process occurs along torturous routes between pores in the porous material but is more planar in the fully dense material. Thus, as is evident in Fig. 7, porosity (especially coarse porosity) assists microcrack linking, although this effect is not as pronounced as the initiation effect.

(4) Defining a macrocrack as crack whose size is sufficiently long so as to cause a measurable decrease in peak load, the data Fig. 7 also show that the porosity accelerates somewhat the fully plastic growth of a macrocrack. This is

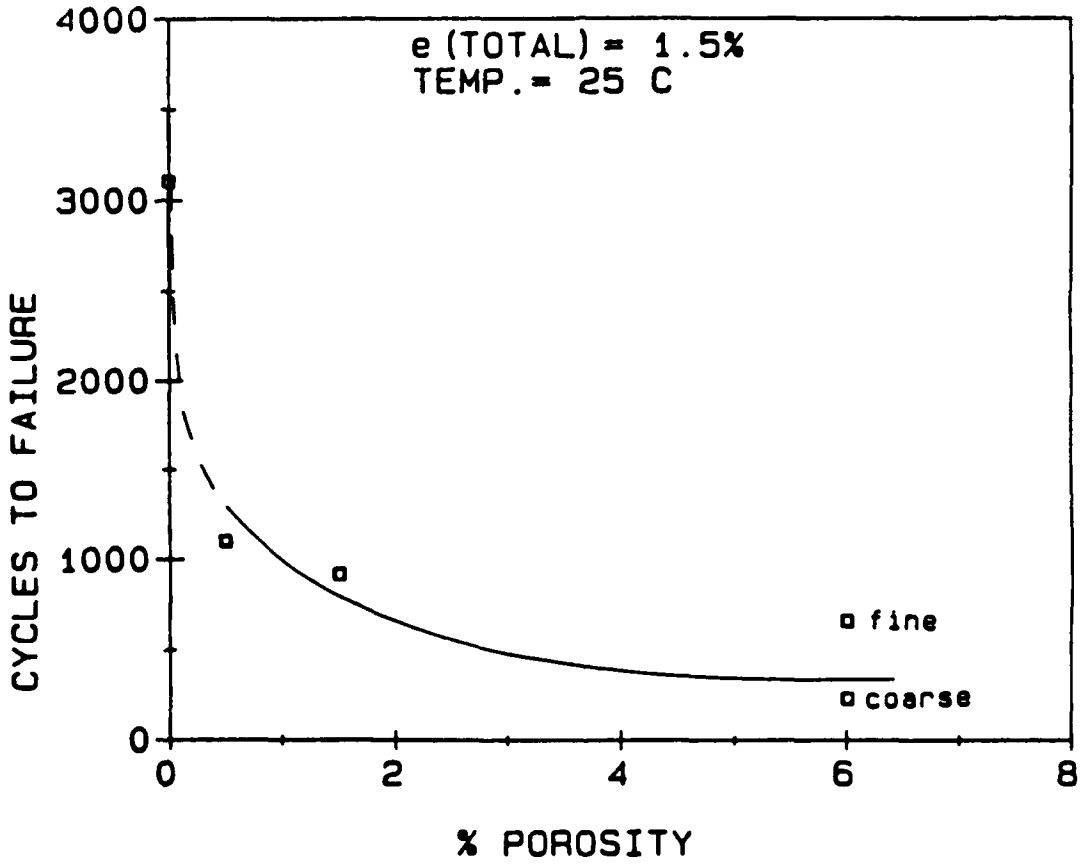


Fig. 6. The number of cycles to failure as a function of porosity condition for powder-processed titanium.

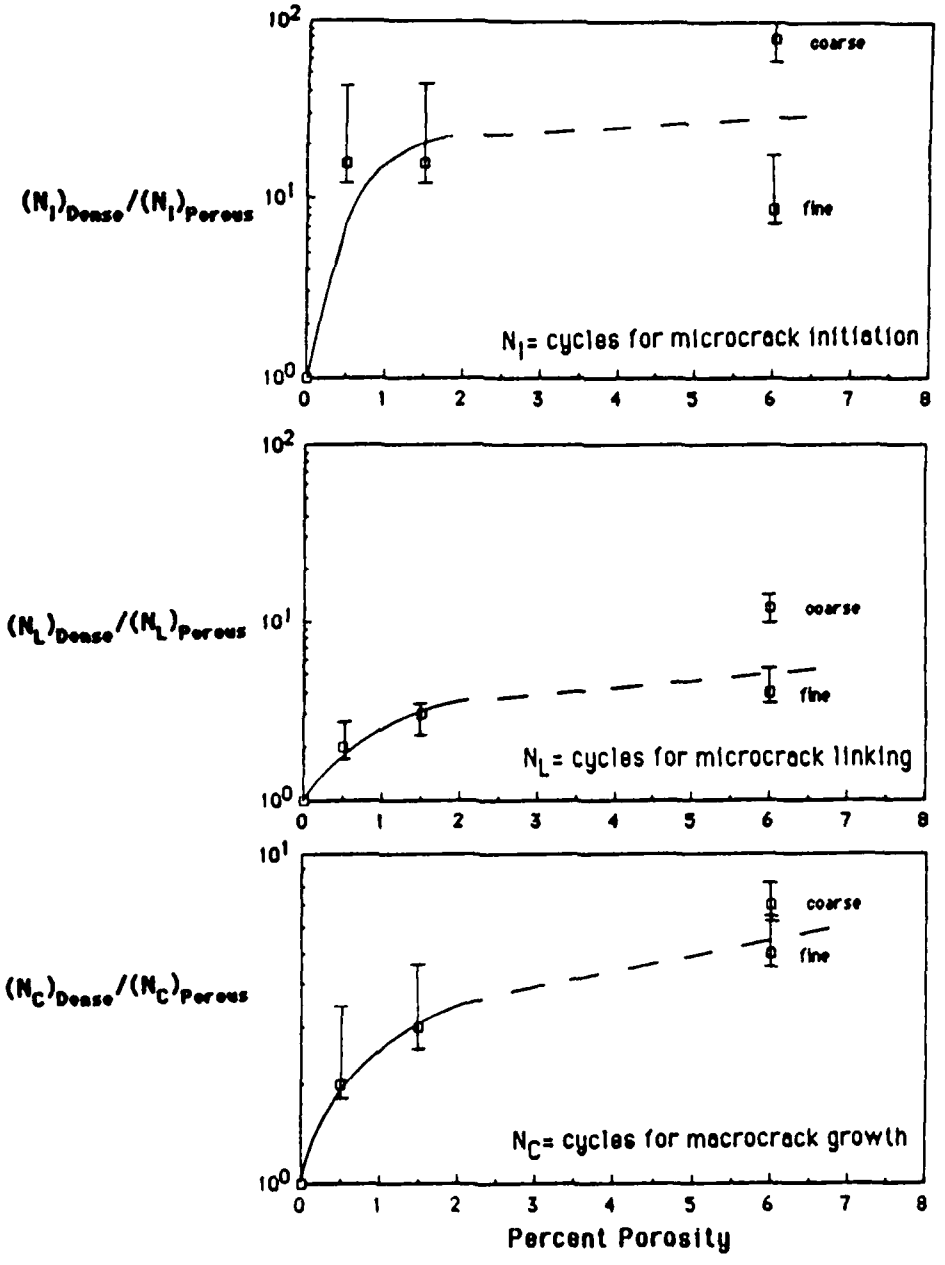


Fig. 7. The number of cycles for each of the LCF failure stages of the fully dense material normalized to the individual failure stages of the porous titanium. The ratios indicate the effect that porosity has on accelerating each of the stages of fatigue failure when compared to the fully dense titanium.

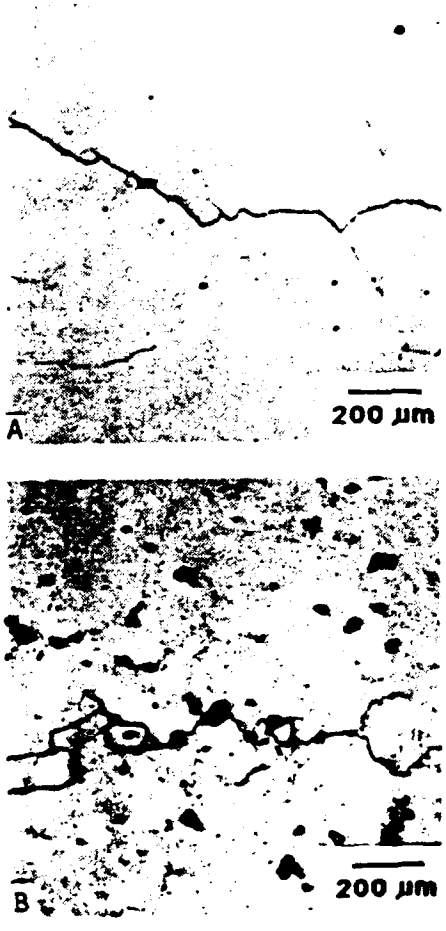


Fig. 8. Surface replicas revealing microcrack link-up for (a) the 0.5% porous (1000 cycles), and the 6% porous titanium (600 cycles). The fatigue axis is vertical.

also evident from fractography which shows extremely tortuous crack growth as the crack links clusters of large pores.

Presently low cycle fatigue testing is being performed at room temperature at a smaller total strain amplitude (.75%). Future work will include low cycle fatigue testing at approximately 400°C in order to examine the effect of a charge in the matrix flow behavior while maintaining constant pore microstructures. In addition, macroscopic modeling of fatigue-induced linking of pores will be performed on specially designed low cycle fatigue specimens having circular holes machined to specific sizes, spacings and orientations.

3. The Deformation of Rapidly Solidified Ti Alloys at Elevated Temperatures [with Steven Kampe, Ph.D., January 1987].

Rapid solidification (RS) techniques have been recently applied to titanium-based alloys designed for high temperature use. These alloys are based on the introduction of a fine, homogeneous dispersion of oxide particles through the internal oxidation of rare-earth alloying additions to the titanium matrix. Several investigators have established the potential of RS in oxide dispersion strengthened (ODS) titanium alloy development through extensive evaluation of the thermal-mechanical stability of candidate materials in the form of ribbons or flakes (see, for example, Ref. 28-34). However, commercial application of titanium based alloys produced via rapid solidification will rely not only on the retention of favorable microstructural features but also on enhanced creep strength following consolidation of the fine-scaled RS product into bulk, usable form.

Despite numerous studies of the microstructural stability of various RS Ti alloys in ribbon form, there has been no systematic study of the high

temperature creep behavior of an ODS titanium alloy formed by RS and consolidated into bulk form. Only a few data are available, and these indicate strengthening over a narrow range of stress/temperature/strain rates.[32] The present work has explored the microstructural evolution and subsequent deformation behavior of rapidly solidified Ti and Ti-Al alloyed with Er additions.[35,36] The following is a brief summary of the principal observations.

When consolidated into bulk form, Ti-Er and Ti-Al-Er alloys produced by rapid solidification techniques retain a fine and homogeneous dispersion of oxide particles within fine grained (3-5 μm) matrices. In the as-consolidated form, the majority of the dispersoids are very fine (average diameter ≃40-80 nm) and generally reside within the interiors of the matrix grains. However, a few large dispersoids (diameter $\geq$ 200 nm) are also present: most of these are located on grain boundaries. Both the dispersoids and fine grains present in the as-processed alloys are extremely resistant to coarsening for high temperature anneals at temperatures near the beta-phase transus temperatures. An increase in grain size is achieved only by heat treatments at temperatures within the beta-phase field; however, this is accompanied by significant dispersoid coarsening. Specifically, the grain size increases by an order of magnitude to 25, 40, and 35 μm following heat treatments of 932°C/2 hr, and Ti-10Al-1Er, respectively; the corresponding dispersoid sizes also increase to 300, 251, and 196 nm (average diameter).

Results from compression testing of the Ti, Ti-Er and Ti-Al-Er alloys over a wide range of conditions indicate that the yield strength of these alloys is sensitive to temperature, strain rate, grain size, and alloy composition. Tests were performed at temperatures ranging from ambient to 775°C, at strain rates ranging from ambient to 775°C, at strain rates ranging from $5\times10^{-5}$ to $1.25\times10^{-3}$ $s^{-1}$ and for fine (3-5 μm) and coarse (25-40 μm) grained material. At room

temperature, solid solution strengthening from both aluminum and interstitial oxygen contributes significantly to the observed strength. Lower strengths in the erbium-containing alloys at room temperature reflect reduced solid solution strengthening due to the depletion of oxygen as a result of the internal oxidation of the erbium to erbia.

Based on the conditions imposed in the present study, the high temperature deformation of the ODS alloys is characterized by "two stage" deformation behavior, with two distinct deformation mechanisms operative over specific ranges of temperature, strain rates, and/or stresses. In the range of higher temperatures and lower strain rates ($\dot{\varepsilon}/D \leq 1 \times 10^{12}\ m^{-2}$), mechanical test data (see Fig. 9) and post-deformation microscopy indicate that grain boundary sliding is the rate-controlling deformation mechanism in the fine grain alloys. Increasing the grain size from 3-4 μm to 25-40 μm enhances the high temperature strength and creep resistance of the strengthened titanium alloys; see Fig. 10. This occurs as a result of: a) a minimization or elimination of grain boundary sliding as the dominant deformation mechanism due to the reduction of grain boundary area, b) an increased density and size of dispersoids residing on grain boundaries, also acting to minimize grain boundary sliding by mechanically "pinning" the boundaries, and c) further precipitation of oxide particles during the high temperature grain growth anneals, thus providing additional particle strengthening capability. The experimental behavior shows good agreement with constitutive equations which model deformation via grain boundary sliding mechanisms.

For conditions of lower temperatures and/or high strain rates, an analysis of the mechanical test data in Figs. 9 and 10 indicates that dislocation creep past obstacles controls the rate of deformation in these alloys. Post-deformation microscopy reveals evidence of significant

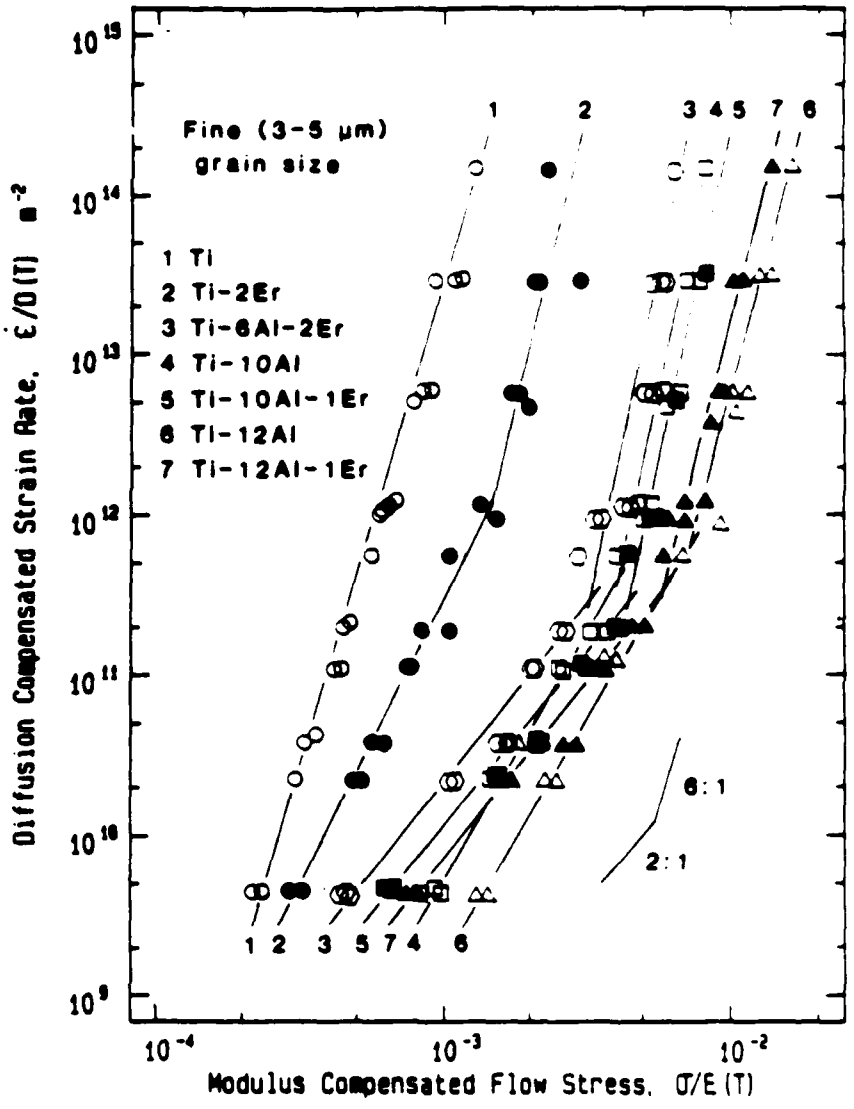


FIG. 9. Summary of results from the alloys in the as-processed, fine grained form showing relative resistance to high temperature deformation.

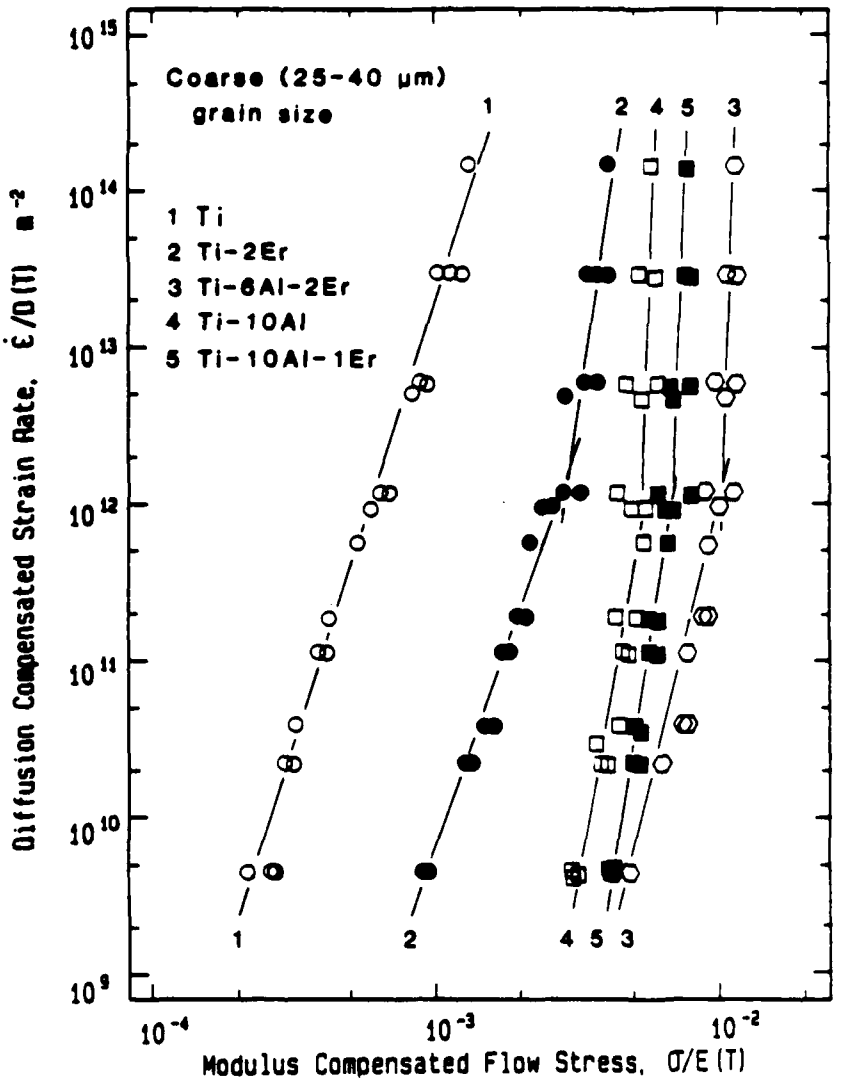


FIG. 10. Summary of results from alloys following grain growth anneals showing relative resistance to high temperature deformation.

dislocation-dispersoid interaction in alloys tested under these conditions of temperature and strain rate ($\dot{\varepsilon}/D \geq 10^{12}\ m^{-2}$). The apparent grain size effect in the dispersoid-containing alloys under these conditions is interpreted to be a result of an increased population of dispersoids which evolve during the high temperature grain growth anneals.

4. On the Influence of Strain-Path Changes on Fracture [with Susan Kestner, M.S., May 1986].

The influence of strain-path changes on the flow behavior of metals, especially with regard to strain-hardening transients, has been the subject of several previous studies (see, for example, ref. 37). These transients can in turn have several effects on the subsequent flow behavior: for example, recently published finite element modeling indicates that the transients can influence strain localization behavior at strains well beyond the transient region[38]. Thus, formability of sheets can be affected significantly even by strain-path changes at comparatively small strains.

In contrast to the above, the effect of strain-path changes on ductile fracture [wherein failure is a result of void nucleation, growth, and linking] has not been examined in detail. Studies based on proportional loading clearly show that the fracture strain for a ductile, microvoid fracture process is a function of both stress state and stain-path. Thus, it would be reasonable to expect that ductile fracture should be a function of changes in strain paths and strain-path history. This study has obtained unique data which indicate that ductile fracture, at least in certain cases, is strongly dependent on changes in strain-paths imposed prior to failure.[39] In particular, a multi-stage deformation sequence involving uniaxial and equibiaxial tension can result in a

significant ductility enhancement when compared to that achieved by proportional straining ($\rho = d\varepsilon_2/d\varepsilon_1 = \text{constant}$, where $\varepsilon_1$ and $\varepsilon_2$ are the major and minor principal strains in the plane of the sheet) to the same final strain state. The effect occurs regardless of whether void nucleation is difficult (pure Ti), or relatively easy (a Ti-H alloy in which hydrides provide sites for void nucleation).

A comparison of the fracture strains after both proportional and non-proportional straining is shown in Figure 11. This figure shows the major and minor principal stains in the plane of the sheet ($\varepsilon_1$ and $\varepsilon_2$, respectively) both after the pre-strain stage and after fracture. Since the pre-strains resulted in nearly uniform deformation of very reproducible magnitude, these data are indicated with a single data point. The fracture strain data, especially when measured on a local scale, show considerably more scatter. In Fig. 11, a final strain state of plane-strain tension may be obtained by either (a) proportional straining, (b) a nonproportional path of uniaxial -> equibiaxial tension, or (c) an equibiaxial -> uniaxial tensile path. As is obvious from Fig. 11 both of the two nonproportional paths result in significant increases in fracture strain at a final strain state of roughly plane-strain tension. The magnitude of the ductility enhancement is sensitive to the strain-path sequence, being more pronounced for the combination of equibiaxial -> uniaxial tension than for uniaxial prestrain followed by equibiaxial tension. The magnitude of the increase is also sensitive to the presence of hydrides, being smaller in the Ti-650H material in which hydrides are present.

On the basis of both damage and strain-hardening considerations, it is not surprising that non-proportional, multi-stage tensile deformation has a significant effect on the total strain to fracture. What is surprising is the relatively large magnitude of the effect, especially in the Ti-30H material, and

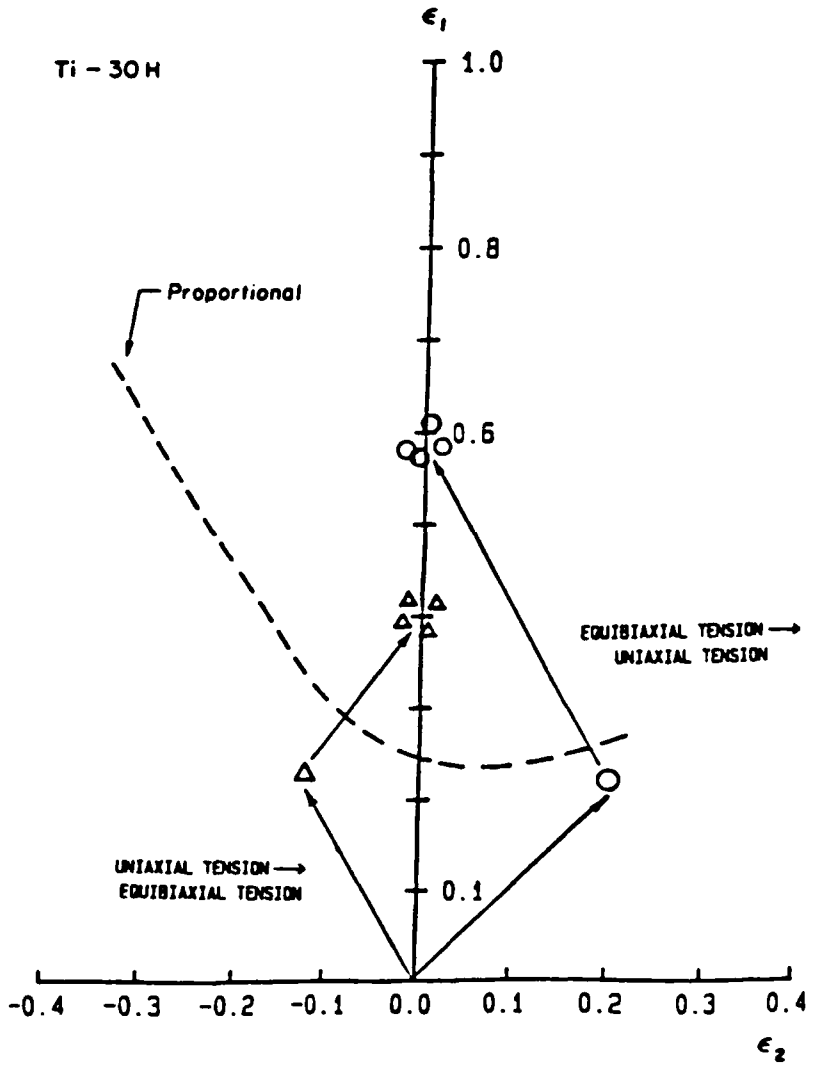


Fig. 11. The influence of strain path on the major and minor principal strains at fracture of titanium sheet containing 30 wt ppm H.

the fact that it is a ductility enhancement. At this time, we do not have a complete explanation for the above effect. From a damage standpoint, one contributing factor may be the large maximum principal stress associated with plane-strain deformation* in this plastically anisotropic sheet. By using multi-stage uniaxial and equibiaxial paths to achieve a final strain state of plane stain, the material avoids being subjected to the large $\sigma_1$ associated with plane-strain tension. This should delay void nucleation and contribute to enhancing ductility, as is observed. However, the magnitude of the effect suggests that other factors are also important. The importance of strain-hardening transients is recognized, but we have neither the appropriate data nor an analysis to predict the effect.

5. Hot Isostatic Pressing of Metallic Powders [with Barbara Lograsso, Ph.D. candidate].

Hot isostatic pressing (HIP) of powders, rapidly solidified ribbons or flakes, or castings is becoming increasingly important as a process to eliminate porosity. In the absence of fundamental studies of HIP, unnecessarily high temperatures and pressures plus long times are commonly used to obtain full density. This may be a particularly important restriction when HIP is used to consolidate rapidly solidified ribbon or powder particles, and low temperature/short times are desired to retard microstructural coarsening.

This study seeks to extend the experimental examination of densification during hot isostatic pressing to engineering materials which are processed by

* $\sigma_1 \simeq 1.4\bar{\sigma}$ for plane strain as compared to $\sigma_1 = 1.0\bar{\sigma}$ in uniaxial tension, assuming the Hill criterion for yielding.

HIP to near-net shape in order to exhibit a good combination of strength and ductility. The work described here concerns hot isostatic pressing experiments of commercially pure titanium in the form of both spherical and angular shaped powders over densities ranging from packing density to full density.[40]

The dependence of the relative density on HIP time and temperature is shown in Figs. 12 and 13 for the -70+100 mesh powders (144-177 μm) in both the spherical PREP and irregular HDH conditions pressed at 34 and 21 MPa. On the basis of these figures, several observations are noteworthy. As expected from previous studies, the density increases very rapidly during the initial stage of densification. This is especially dramatic for the angular powders which have initial packing densities of 42 or 54% for the fine and coarse particles, respectively. Comparing Figs. 12 and 13 shows that densification is pressure dependent such that the rate of density increase is more rapid at the higher pressure, as is expected. For densities less than 0.95, at a given HIP time the relative density of the angular Ti is slightly higher that that for the spherical powder. This occurs despite the low initial packing density. At 34 MPa for hold times greater than 1 hour, the relative density for both powders is greater than 95%. In these cases, the relative density of both spherical and angular Ti powders are within experimental error of each other. This result agrees with a previous experimental observation[42] of the densification of powders by particle deformation; as the angular particles are flattened together at high densities (>0.95), the absence of further particle rearrangement causes the densification behavior to approach that of spherical particles. It should be noted that the compacts containing mixes of different sizes of spherical powders densify at the same rate as monosized powders. This is contrary to a recent analysis which predicts enhanced densification for mixes of particle sizes.[41]

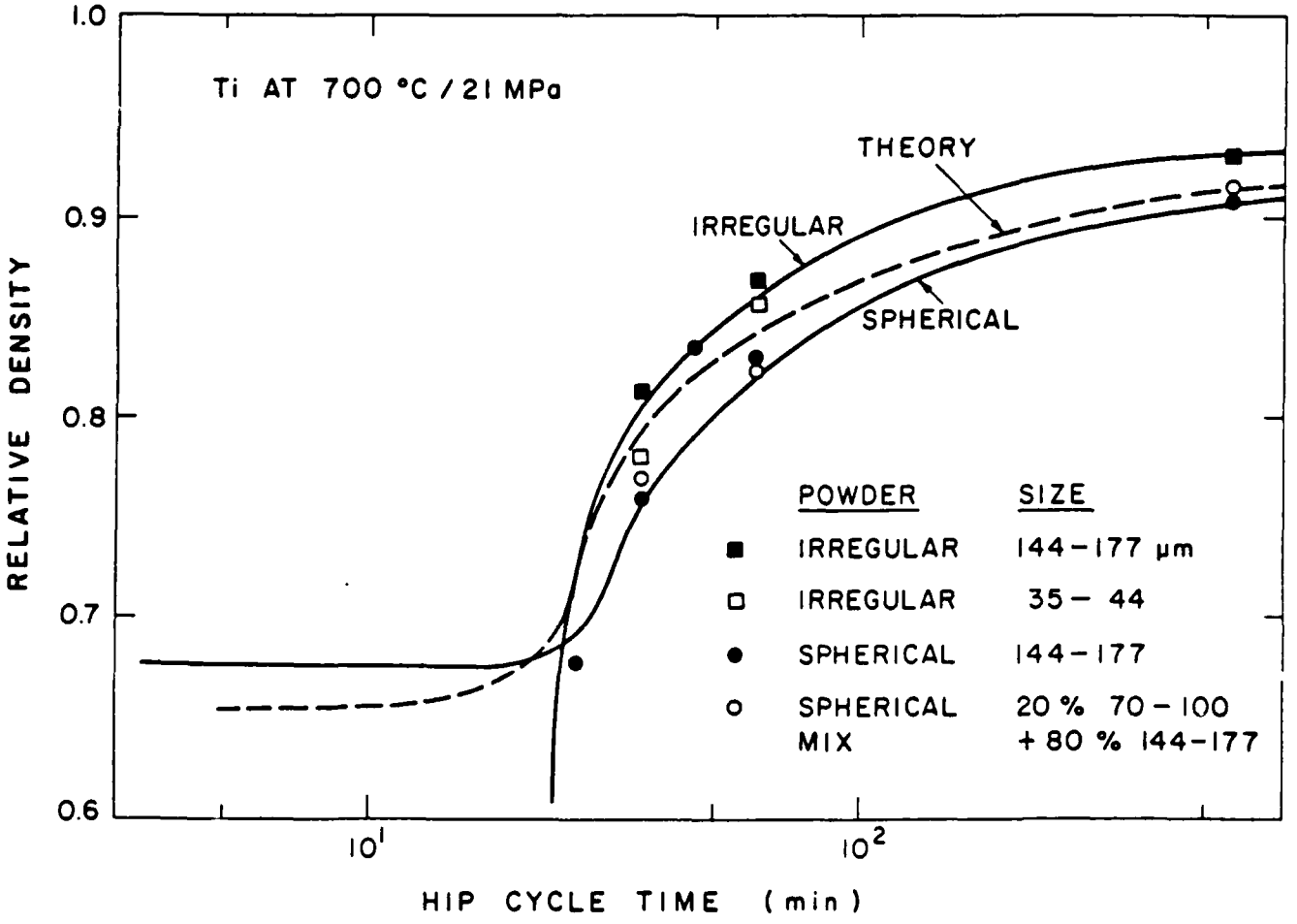


Fig. 12. The densification of Ti powders during HIP at 700°C and 21 MPa. Predicted behavior based on the theoretical analysis of Arzt et al[3] is indicated.

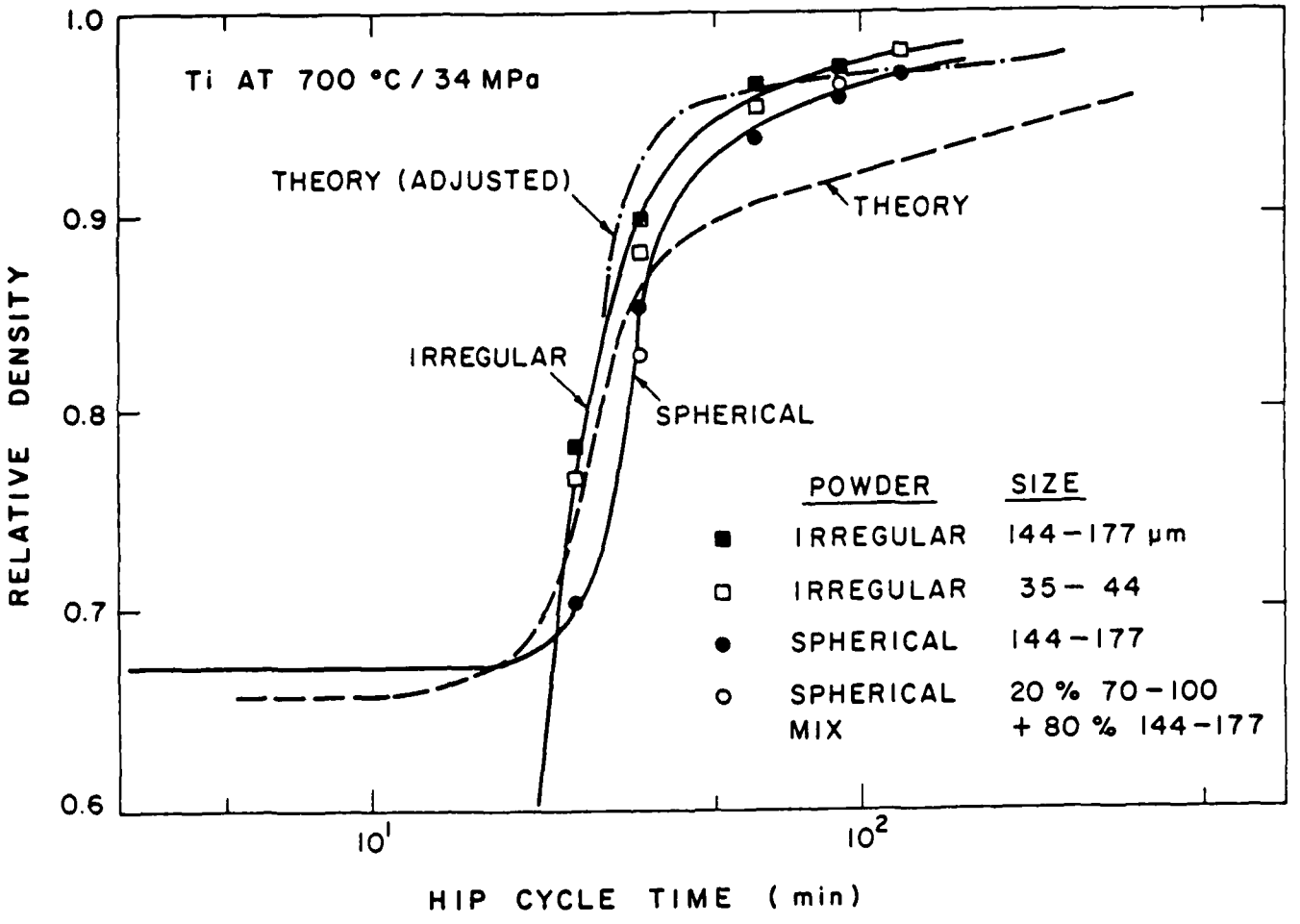


Fig. 13. The densification of Ti powders during HIP at 700°C and 34 Mpa. The predicted behavior is also shown for the Arzt et al model for the case where Stage I/II transition occurs at 0.90 and as adjusted to a 0.95 transition.

The densification rate equations derived by Arzt et al.[43] have been used to calculate predicted densities for the HIP cycles used at 21 MPa and 34 MPa at 700°C. Figs. 12 and 13 show the predicted results of this theory as compared to experimental data. Agreement is very good between experimental densities of screened powder and predicted densities based upon the model of densification of mono-size spheres HIP'd at 21 MPa. For this HIP condition the initial stage of densification should dominate the analysis since densification remains less than ~91% of theoretical density. As is evident in the microstructures of the compacts, in this initial stage the powder particles can still be distinguished from one another for both the angular and spherical titanium powders. Even at relative densities in the range of 91-92%, the absence of triple lines[42] in the pore microstructure suggest continuous porosity. Therefore the microstructures of the compacts do not show the transition from compacting spheres (initial stage) to a homogeneous solid containing isolated pores until densities of ~96% theoretical have been achieved. Thus, agreement between theory and experimental data is good at 21 MPa because the density range is limited to roughly 90% or less. However at 34 MPa, good agreement between theory and experiment is obtained for densities in excess of 90% only if the transition between Stages I and II is increased to a density of 95%. This is consistent with the observation of pore microstructures and measurements of interconnected porosity which indicate isolated porosity at ~96% density. Finally, it should be noted that despite the fact that the Arzt et al model[43] has been developed for monosized spheres, it provides a very good estimate for the densification of mixes of particle sizes of spherical powders as well as for the irregular powders used in the present study.

ACKNOWLEDGMENT

This research was supported by the Office of Naval Research through Contract No. N00014-86-K-0381.

REFERENCES


1. A. R. Cox, J. B. Moore, and E. C. Van Reuth in Superalloys: Metallurgy and Manufacture, Claitor's Press, Baton Rouge, LA), p. 45, 1976.

2. M. Cohen, B. H. Kear, and R. Mehrabian, in Proc. of 2nd Int. Conf. on Rapid Solidification, (Claitor's Press, Baton Rouge, LA), p. 1, 1980.

3. N. J. Grant, J. of Metals 35, 20, 1983.

4. S. M. L. Sastry, T. C. Peng, and J. E. O'Neal, in Proc. Int. Powder Met. Conf., Toronto, June, 1984.

5. E. A. Dubensky and D. A. Koss in Aluminum Alloys Their Physical and Mechanical Properties, Vol. II, (Engineering Materials Advisory Services, U.K.) 1986, p. 999.

6. E. A. Dubensky and D. A. Koss, Metall. Trans. (in print).

7. P. E. Magnusen, D. A. Koss, and E. M. Dubensky, ONR Tech. Rep. No. 5, Contract No. N00014-86-K-0381, February 1987.

8. K. S. Chan, D. A. Koss, and A. K. Ghosh, Metall. Trans. A 15A, 323 (1983).

9. H. Yamamoto, Int. J. Frac. 14, 347 (1978).

10. M. Sage, J. Pan, and A. Needleman, Int. J. Frac. 19, 163 (1982).

11. B. I. Edelson, Trans. ASM 56, 89 (1963).

12. R. J. Bourcier, R. E. Smelser, O. Richmond, and D. A. Koss, Int. J. F rac. 24, 289 (1984).

13. F. A. McClintock, J. of Appl. Mech. 35, 363 (1968).

14. A. Needleman, J. of Appl. Mech. 39, 964 (1972).

15. M. Nagumo, Acta Metall. 21, 1661 (1973).

16. S. I. Oh and S. Kobayashi, Tech. Rep. AFML-TR-76-61 (1976).

17. P. F. Thomason, Acta Metall. 29, 763 (1981).

18. P. F. Thomason, Acta Metall. 30, 279 (1982).

19. V. Tvergaard, Int. J. Frac. 17, 389 (1981).

20. P. F. Thomason, Acta Metall. 33, 1079 and 1087 (1985).

21. L. M. Brown and J. D. Embury, in Proc. 3rd Int. Conf. Strength of Metals and Alloys, 1973, p. 164.

22. R. A. Tait and D. M. R. Taplin, Scripta Met 13, 77 (1979).

23. G. LeRoy, J. D. Embury, G. Edward and M. F. Ashby, Acta Metall. 29, 1509 (1981).

24. P. E. Magnusen, J. K. Lee, and D. A. Koss, unpublished research.

25. G. LeRoy and J. D. Embury in Formability (TMS-AIME, Warrendale, PA), p. 183, 1976.

26. K. M. Vedula and R. W. Heckel in Modern Developments in Powder Metallurgy (MPIF, Princeton), 1981, p. 759.

27. R. Haynes, The Mechanical Behavior of Sintered Alloys (Freund Publishing House, London), 1981.

28. H. B. Bomberger and F. H. Froes, Titanium Rapid Solidification Technology (Proc Conf), New Orleans, March 2-6, 1986, 21-43.

29. S. H. Whang, J. Mat. Sci., 21, 1986, 2224-2238.

30. S. M. L. Sastry, D. M. Bowden, and R. J. Lederich, Titanium Science and Technology (Proc Conf), Vol. 1, Munich, Sept. 10-14, 1984, 435-441.

31. D. G. Konitzer, B. C. Muddle, H. F. Fraser, and R. Kirchheim, ibid., 405-410.

32. S. M. L. Sastry, P. J. Meschter, and J. E. O'Neal, Met. Trans. A, 15A, 1984, 1465-1484.

33. S. M. L. Sastry, P. J. Meschter, and J. E. O'Neal, J. Metals, 35 (9), 1983, 21-28.

34. S. H. Whang, J. Metals, 36 (4), 1984, 34-40.

35. S. L. Kampe and D. A. Koss in Enhanced Properties in Structural Metals via Rapid Solidification, (ASM, Metals Park) (in print).

36. S. L. Kampe, Ph.D. Thesis, Michigan Technological Univ., 1987.

37. R. H. Wagoner and J. V. Laukoniz, Metall. Trans. A, 14A, 1487 (1983).

38. K. Chung and R. H. Wagoner, Metall. Trans. A 17A, 1001 (1986).

39. S. C. Kestner and D. A. Koss, Metall. Trans. A (in print); see also Tech. Rep. No. 1, Office of Naval Research Contract N00014-86-K-0381, August 1986.

40. B. K. Lograsso and D. A. Koss, Tech. Rep. No. 4, Office of Naval Research Contract N00014-86-K-0381, January 1987.

41. S. V. Nair and J. K. Tien, Metall. Trans. A 18A, 97 (1987).

42. H. F. Fischmeister and E. Arzt, Powder Met, 26, 82 (1983).

43. E. Arzt, M. F. Ashby, and K. E. Easterling, Metall. Trans. A 14A, 211 (1983).

END

9-87

DTIC